Article

Not peer-reviewed version

Chemical Vapor Deposited 2D MoN Nanosheets as Stable and Uniform Surface Enhanced Raman Scattering Substrate with Thickness Dependent Sensitivity

Hongrong Wu *, Maolin Tang , Pinsen Tong , Yang Hang , Junhua Zhao

Posted Date: 7 December 2023

doi: 10.20944/preprints202312.0498.v1

Keywords: two-dimensional materials; surface enhanced Raman scattering; MoN nanosheets; thickness dependent sensitivity; stability

Article

Chemical Vapor Deposited 2D MoN Nanosheets as Stable and Uniform Surface Enhanced Raman Scattering Substrate with Thickness Dependent Sensitivity

Hongrong Wu *, Maolin Tang, Pinsen Tong, Yang Hang and Junhua Zhao *

Jiangsu Key Laboratory of Advanced Food Manufacturing Equipment and Technology, Institute of Strength and Multi-scale Mechanics of Mechanical Structures, School of Mechanical Engineering, Jiangnan University, 214122 Wuxi, PR China

Abstract: Two-dimensional (2D) materials show advantages as surface enhanced Raman scattering (SERS) substrate over traditional noble metals, such as chemically inert flat surface and uniform SERS signals. However, due to the low density of free electrons of 2D materials, the enhancement mechanism is mainly restricted to chemical enhancement instead of electromagnetic enhancement, resulting a relatively low enhancement factor. In this work, we reported a sensitive 2D SERS substrate based on chemical vapor deposited MoN nanosheets with electromagnetic enhanced mechanism. The maximum enhancement factor can be 3×10^5 with a limit of detected concentration of 4×10^{-8} M, which is comparable to those noble metal SERS substrates without hot spots. The MoN nanosheets show strong surface plasmon resonance in the visible range as evidenced by the UV-vis absorption spectroscopy and first principle calculation. The MoN nanosheets SERS substrates exhibit excellent Raman signal uniformity within the nanosheets. Meanwhile, distinct thickness dependent sensitivity was observed in the MoN nanosheets, higher sensitivity can be achieved by decreasing the thickness of the nanosheets. Furthermore, the MoN nanosheets SERS substrate also show high thermal stability, which can be annealed in air for more than 300℃ and maintain its SERS activity. The high stability of MoN nanosheets allows it to be reused for 20 cycles without obvious signal decay. The high sensitivity, stability, reusability and Raman signal uniformity, makes MoN nanosheets an ideal 2D SERS substrate for practical applications.

Keywords: two-dimensional materials; surface enhanced Raman scattering; MoN nanosheets; thickness dependent sensitivity; stability

1. Introduction

Surface-enhanced Raman scattering (SERS) has emerged as a powerful analytical technique in various research fields such as electrochemistry, catalysis, biology and materials science, capable of enhancing the Raman signals by several orders of magnitude[1, 2]. The SERS effect can be mainly attributed to two mechanisms. One is the electromagnetic mechanism, which involves the amplification of local electromagnetic fields due to surface plasmon resonance[3-7]. The other one is the chemical mechanism, which origin from the charge interaction between the substrate and adsorbate[8-10]. The substrate plays a vital role in the SERS applications. Noble metals such as gold and silver can be used as sensitive SERS substrate based on the electromagnetic mechanism [11-15], which can enhance the Raman signal for 10^5-10^{12} time[16]. However, noble metals have disadvantages such as high cost, high surface activity and poor biological compatibility[17-19]. Recently, many non-metal SERS substrates with nanostructures have drawn much attention due to their low cost, high stability and inert surface, such as CuO nanospheres[20], TiO_2 nanocrystals[21], Fe_2O_3 nanoparticles[22] and MoO_2 nanocrystals[23]. The SERS substrates with nanoparticles or nanostructures configuration often surfer from the reproducibility of the Raman signals, because the geometry of the absorbed molecules, as well as the distribution of the molecules, can be quite different in different spots of the substrate. The emerging

 doi:10.20944/preprints202312.0498.v1

SERS substrates based on 2D materials provides a new opportunity for uniform SERS signals, due to their atomic flat surface which enables the uniform absorption of molecules. Graphene, boron nitride and transition metal dichalcogenides can be used as SERS substrate via chemical mechanism[24-26]. However, the sensitivity of the SERS substrates based on 2D materials is relatively low. It is highly demanded to develop new SERS substrates with high sensitivity, low cost, good stability and high Raman signal uniformity[27].

Molybdenum nitride (MoN) has garnered significant attention due to its high concentration of free electron density, excellent catalytic property, and outstanding mechanical performance[28-33]. Recently, various structures of MoN were synthesized as SERS substrates. For example, Guan et al. have successfully prepared a thermally stable MoN nanosheet using a low-temperature solution method. [34] Song et al. prepared a type of porous hexagonal prism-shaped MoN nanocrystals, which possess extremely high porosity and excellent antioxidation properties.[35] Du et al. achieved MoN hollow spheres with a high specific surface area using microwave heating[36]. While these methods, mostly based on solution processes, can yield MoN with high enhancement factors. The nanoparticle or nanostructure configuration of the MoN making it challenging to control the uniformity of the substrates. Defects in MoN nanostructures and aggregation of the MoN nanoparticles are also problems. Meanwhile, the reusability of those substrates based on nanostructures can hardly be achieved.

In this work, 2D MoN nanosheets was synthesized by chemical vapor deposition (CVD). The MoN nanosheets present sensitive SERS activity, with a maximum enhancement factor of 3×10^5 and a limit of detection of 4×10^{-8}M. The mechanism for the SERS effect of MoN nanosheets was attributed to surface plasmon resonance, as evidenced by the first principle calculation and UV-visible absorption spectroscopy. Thanks to its planar structure, the Raman signals on MoN nanosheets show excellent uniformity within the nanosheets. Distinct thickness dependent SERS sensitivity was also observed in the MoN nanosheets, higher sensitivity can achieve in thinner nanosheets. Meanwhile, the MoN nanosheets exhibit high thermal stability, which can be annealed in air for more than 300℃ and maintain its SERS activity. The high stability of MoN nanosheets makes it possible to be used as reusable SERS substrate, no obvious decay of the Raman intensity was observed after 20 reuse cycles.

2. Materials and Methods

Preparation of the MoO_2 nanosheets: Place a small amount of MoO_3 powder (5 mg) in a quartz boat, with a SiO_2/Si substrate positioned directly above the MoO_3 powder. Then put the quartz boat and the substrate into a high-temperature tube furnace. Prior to growth, evacuate the furnace to a pressure of 1 Pa, then close the vacuum pump and inject high-purity nitrogen gas into the tube until the pressure reaches atmospheric pressure. Once this pressure is attained, proceed to close the vacuum pump and introduce high-purity nitrogen gas into the tube until the pressure reaches atmospheric levels. To maintain a continuous flow of nitrogen gas, open the air valve and set the flow rate to 20 sccm. Gradually heat the tube furnace at a rate of 20 ℃/min until it reaches a temperature of 600 ℃. Subsequently, within a span of 7 minutes, increase the temperature to 825 ℃ and uphold this level for 5 minutes, enabling the growth of MoO_2 nanosheets. Finally, quickly cool down the tube furnace to room temperature to finish the growth of MoO_2 nanosheets.

Nitridation of MoO_2 nanosheets to prepare MoN nanosheets: Using urea as the nitrogen source, place urea and the prepared MoO_2 nanosheets separately in the temperature zones 1 and 2 of the tube furnace (**Figure 1**a). Evacuate the furnace before the nitridation, then continuously introduce high-purity nitrogen gas at a flow rate of 20 sccm to maintain low pressure inside the tube. Heat temperature zone 1 of the tube furnace at a rate of 20 ℃/min up to 600 ℃, then increase the temperature to 750 ℃ within 5 minutes, while simultaneously raising temperature zone 2 to 90 ℃ within 5 minutes. Maintain these temperatures for 60 minutes to ensure the complete nitridation of MoO_2 nanosheets. Finally, open the tube furnace and quickly cooled down to room temperature to finish the growth. In the meantime, adjusting the nitrogen gas flow rate to 400 sccm to remove the excess reactants.

Preprints (www.preprints.org) | NOT PEER-REVIEWED | Posted: 7 December 2023 doi:10.20944/preprints202312.0498.v1

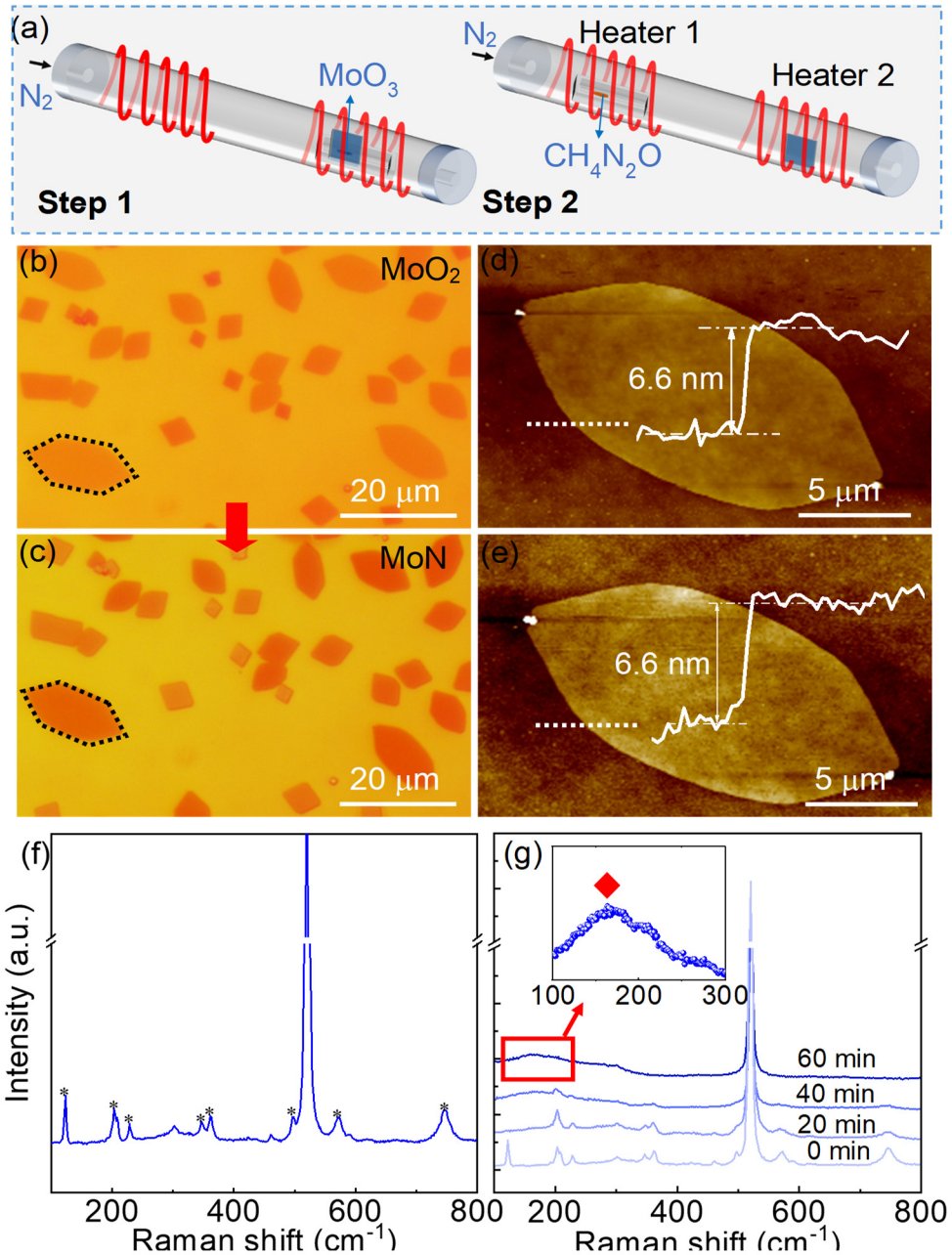

Figure 1. Growth and characterization of MoN nanosheets. (a) Schematic illustration of the two-step CVD growth of the MoN nanosheets. (b) Optical microscopy image of the MoO_2 nanosheets. (c) Optical microscopy image of the MoN nanosheets. (d) AFM characterization of a MoO_2 nanosheet corresponding to the hexagonal dashed box in b. the white curve is the height profile along the white dotted line, indicating the thickness of the nanosheet is 6.6 nm. (e) AFM characterization of the MoN nanosheet after nitridation. The white curve is the height profile along the white dotted line, indicating the thickness of the nanosheet is 6.6 nm. (f) The Raman spectra of MoO_2 nanosheets. (g) Raman spectra evolution of the nanosheets with the increase of the nitridation time, the insert image demonstrates the characteristic Raman peak of MoN at near 160 cm^{-1}.

Calculation of the enhancement factors: The enhancement factors were calculated using the following equations:

$$EF = \frac{I_{surf} / N_{surf}}{I_{bulk} / N_{bulk}} \quad (1)$$

 doi:10.20944/preprints202312.0498.v1

$$N_{surf} = \mathrm{N_A} n S_{Irr} / S_{dif} \quad (2)$$

$$N_{bulk} = \rho S_{Irr} h \mathrm{N_A} / M \quad (3)$$

Where I_{Surf} is the average intensity of the enhanced Raman peaks on MoN SERS substrate. I_{Bulk} is the average intensity of the regular Raman peaks on SiO_2/Si. N_{Surf} is the quantity of R6G molecules in the surface-enhanced Raman spectroscopy test. N_{Bulk} is the quantity of R6G molecules in the regular Raman spectroscopy test. The value of N_{Surf} can be estimated by Equation 2, where N_A is Avogadro's constant (6.0×10^{23}), n is the number of moles of R6G molecules, S_{Irr} is the area of the laser spot (approximately a circle with a diameter of 5 μm), S_{dif} is the diffusion area of the R6G solution on the substrate. To calculate the enhancement factor of the MoN substrate, A 5 μL drop of R6G solution was placed on the SiO_2/Si substrate with MoN nanosheets. After the substrate is dried, a circular spot with a diameter of approximately 3.7 mm is formed. The average Raman peak intensity from seven randomly selected MoN nanosheets are calculated to reduce testing errors. The value of N_{Bulk} can be estimated using Equation 3, where ρ is the density of the bulk R6G (1.2 g/cm^3), h is the laser penetration depth (approximately 5 μm), M is the molecular mass of R6G.

The reusability test of MoN nanosheets: R6G solution with concentration of 10^{-6} M was used to verify the reusability of the MoN nanosheets. The MoN nanosheets was immerging in the solution for 20 min to absorb R6G molecules. The Raman spectra was collected using 532 nm laser. After which the R6G molecules was removed by washing in the methyl alcohol. The Raman spectra of the MoN substrate was taken after removing the molecules, no characteristic Raman peaks of R6G was found as shown in **Figure S**7.

3. Results and Discussion

3.1. Preparation and Characterization of MoN Nanosheets

A two-step CVD process was used to prepare the MoN nanosheets on SiO_2/Si substrates. Firstly, MoO_2 nanosheets were synthesized by atmospheric pressure CVD using MoO_3 powder as precursor in a high-temperature tube furnace (**Figure 1**a). Then the as-grown MoO_2 nanosheets was replaced in the high-temperature tube furnace with two temperature zones for nitridation to prepare the MoN nanosheets, where urea was used as a nitrogen source. Details of the synthesis process can be found in the Experimental Section and **Figure S**1. **Figure 1**b illustrates the optical image of the MoO_2 nanosheets, most of which are in the shape of parallelograms and hexagons. The standard geometric configuration of the nanosheets indicates that the nanosheets are single crystals. As shown in **Figure 1**c, the nanosheets maintain their original shape after nitridation, while the color of the MoN nanosheets slightly deepens compare to the MoO_2 nanosheets. As the thickness of the nanosheets almost remains unchanged (~6.6 nm) after nitridation (**Figure 1**d-e), the color variation of the nanosheets indicates that the refractive index of the nanosheets have changed after nitridation[37], which can regard as an earlier evidence of the successful synthesis of the MoN nanosheets. To further confirm that, Raman spectroscopy characterization of the nanosheets was carried out before and after the nitridation process. As illustrated in **Figure 1**f, typical Raman peaks of MoO_2 nanosheets were observed at 124, 208, 230, 347, 363, 498, 570 and 746 cm^{-1}.[7] With the increasing of the nitridation time, those typical peaks of MoO_2 nanosheets gradually vanished (**Figure 1**g), with a new Raman peak emerging at near 160 cm^{-1}. The new Raman peak belongs to MoN, which is consistent with previous report.[38] The results confirmed the successful preparation of the MoN nanosheets.

The as-grown MoN nanosheets are metallic material with good conductivity. As illustrate in **Figure 2a**, the band structure of MoN nanosheet was calculated by density functional theory, no bandgap was observed at the Fermi level. The high density of states (DOS) found at the Fermi level **(Figure 2b**) indicates the intrinsic metallic property of the MoN nanosheets. To further confirm the metallic characteristic, the current-voltage (I-V) curves of the MoN nanosheets under different temperature were measured (**Figure S2**). The resistivity of the MoN nanosheets are between 6-10×10^{-8} Ω/*m*, which is comparable to that of metals. Meanwhile, the resistivity increases with the increasing

Preprints (www.preprints.org) | NOT PEER-REVIEWED | Posted: 7 December 2023 doi:10.20944/preprints202312.0498.v1

of the temperature. The linear temperature dependence of the resistivity is highly consistent with metals. The high carrier density of MoN nanosheets enable it to support surface plasmon resonance at visible range[39]. As indicated in the UV-vis spectroscopy of the nanosheet in **Figure 4d**, a distinct absorption band around 500 nm was observed, which can be attributed to the surface plasmon resonance of the MoN nanosheets[35]. The absorption band slightly red shifts with an increase in intensity upon the increasing of the nitridation time. As the absorption band is near 532 nm, one of the mostly used commercial laser wavelength in Raman spectroscopy, the MoN nanosheets are hopefully to be used as surface enhanced Raman scattering substrate.

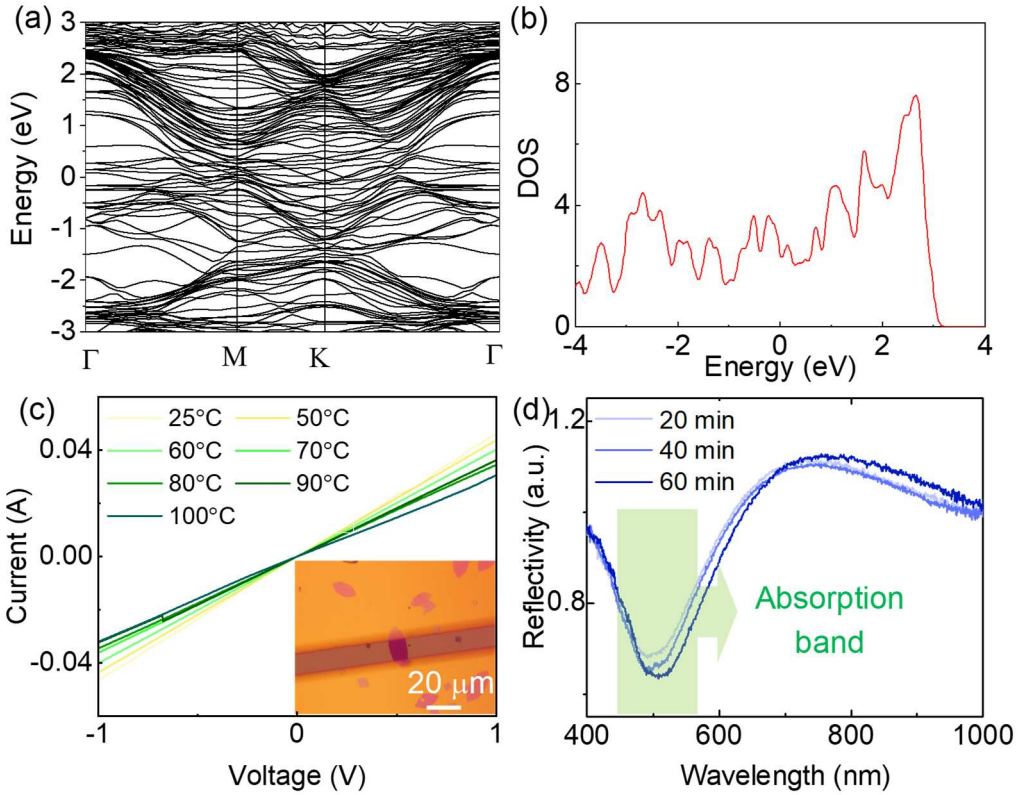

Figure 2. Physical properties of the MoN nanosheets. (a) Band structure of MoN nanosheets obtained by first principle calculation. (b) Density of states at the Fermi level. (c) I-V curves of MoN nanosheets under different temperature, the insert is the optical image of the device, the scale bar is 10 m. (d) UV-vis absorption spectroscopy of MoN nanosheets with different nitridation time.

3.2. SERS Property of the MoN Nanosheets

To investigate the SERS performance of MoN nanosheets, a commonly used Rhodamine 6G (R6G) molecules were chosen as the Raman probe. Before the Raman spectroscopy collection, the SiO_2/Si substrates with MoN nanosheets were immersed in R6G solutions with concentrations ranging from 10^{-3} to 10^{-8} M for 20 minutes to adsorb R6G molecules, after which the samples were dried by high-speed nitrogen flow. The Raman spectroscopy was collected using 532 nm laser, with the laser spot located in the middle of the nanosheets. As shown in **Figure 3**a, no characteristics Raman peaks were detected on the SiO_2/Si substrate. However, distinct Raman peaks of R6G molecules locate at 612 (R1), 772 (R2), 1363 (R3), and 1651 (R4) cm^{-1} were observed on MoN nanosheets, indicating the excellent SERS activity of MoN nanosheets. The Raman peaks R1 and R2 are assigned to the in-plane and out-of-plane bending modes of the carbon and hydrogen atoms in the xanthenes skeleton, Raman peaks R3 and R4 are assigned to the aromatic C-C stretching vibration modes.[40]

Preprints (www.preprints.org) | NOT PEER-REVIEWED | Posted: 7 December 2023 doi:10.20944/preprints202312.0498.v1

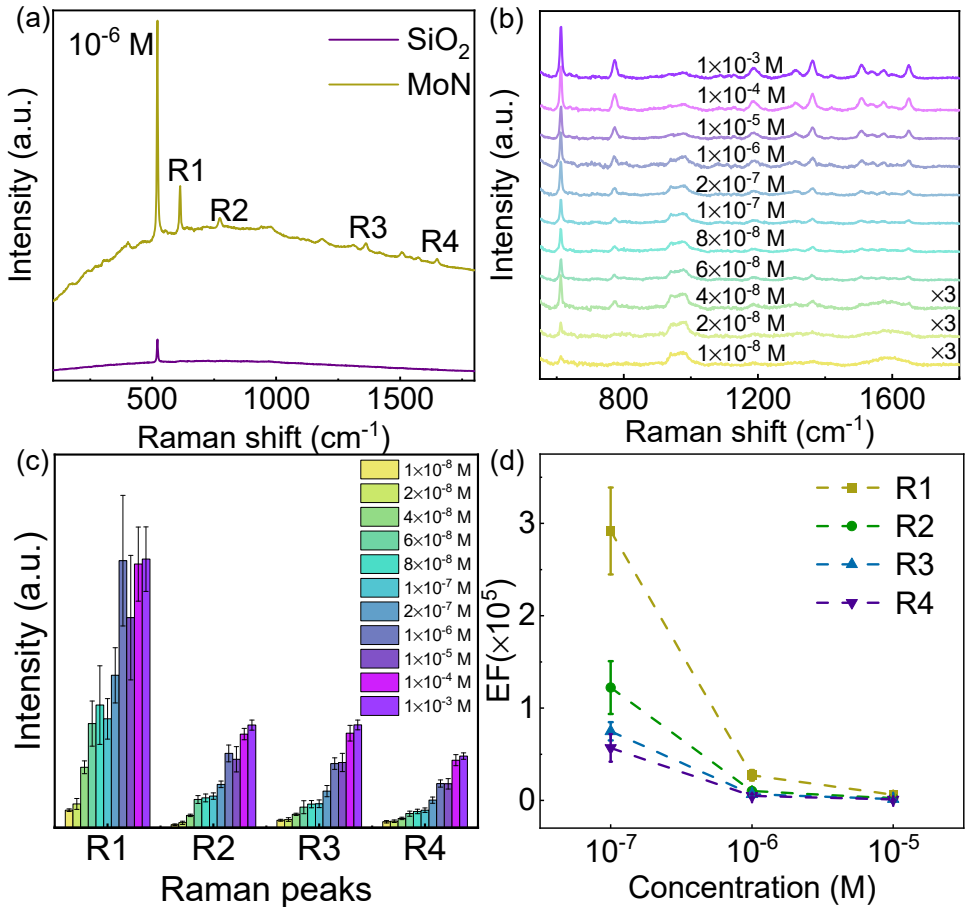

Figure 3. SERS property of MoN nanosheets. (a) Raman spectra of R6G molecules adsorbed on SiO_2/Si and MoN after soaking in the R6G solution with a concentration of 10^{-6} M. (b) Raman spectrum of R6G molecules adsorbed on MoN nanosheets by soaking in the R6G solution with various concentration. (c) The intensity of four typical Raman peaks of R6G molecules extracted from (b). (d) The enhancement factor of four typical Raman peaks of R6G at different concentration levels.

In order to further reveal the SERS effect of the MoN substrate, the Raman spectra of R6G molecules at different concentrations on the MoN substrate were studied. As shown in **Figure 3**b, the Raman signal intensity of the R6G decreases with the decreasing of concentration. When the concentration is as low as 4×10^{-8} M, all the characteristic peaks of R6G molecules can be identified. Therefore, the MoN nanosheets SERS substrate can achieve a minimum concentration of detection of 4×10^{-8} M. In addition, the characteristic peak R1 can be identified even when the concentration further decreases to 1×10^{-8} M. The correlation between the intensity of the four characteristic peaks of R6G molecules and the concentration of the R6G solution was extracted, as shown in **Figure 3**c. It can be observed that the intensity of the Raman peaks increases as the concentration increases and eventually saturated at higher concentration, which can be explained by the Brunauer–Emmett–Teller theory. Furthermore, the enhancement factors of the MoN substrate were calculated by taking the ratio of the Raman intensity of the four characteristic peaks of R6G on MoN substrate and that of bulk R6G (Details in Experimental Section)[23]. The calculation results are shown in **Figure 3**d. The enhancement factors of the four characteristic peaks decrease with the increase of the concentration of R6G solution. The enhancement factor can reach 3×10^{5} when the concentration is 10^{-7} M, which is comparable to noble metal SERS substrate without hot spots[40]. Under the same concentration, the enhancement factors of Raman peaks R1, R2, R3, and R4 decrease in sequence. The difference in the enhancement factors of various characteristic Raman peaks can be ascribed to the binding and geometry of R6G molecules absorbed on the MoN nanosheet surface.[41]

Preprints (www.preprints.org) | NOT PEER-REVIEWED | Posted: 7 December 2023 doi:10.20944/preprints202312.0498.v1

3.3. Raman Signal Uniformity of the MoN Nanosheets

In addition to the sensitivity, the Raman signal uniformity is another important factor for SERS substrate. Unlike those SERS substrates with nanoparticles or rough surface, the 2D configuration of the MoN nanosheets enable the uniform absorption of the probe molecules.[42] Not only the number of the absorbed probe molecules on the surface of MoN nanosheets can be more uniform. Moreover, the geometry of the molecular absorbed on a flat surface can also be more coincident, resulting a cleaner SERS signals. To illustrate the signal uniformity of the MoN nanosheets, methyl violet was used as the probe molecules to avoid the resonant Raman scattering. A large MoN nanosheet was selected as the SERS substrate to perform Raman mapping test. As shown in **Figure 4**a, the Raman mappings based on three typical Raman peaks of the methyl violet located at 914, 1182 and 1622 cm^{-1} show excellent uniformity within the MoN nanosheets. To illustrate it more clearly, the Raman spectra along the green dotted line in **Figure 4**a are plotted in **Figure 4b**. The characteristic Raman peaks of methyl violet are invisible on SiO_2 substrate as shown by the front clarets line. Moreover, the relative standard deviations (RSD) of the three typical Raman peaks are calculated by randomly selected 50 points within the MoN nanosheets, as shown in **Figure 4(c-e)**, where the RSD for three typical Raman peaks are 4.4 %, 5.4% and 5.7%, respectively. The results indicate that the MoN nanosheets can be used as SERS substrate with high uniform SERS signals.

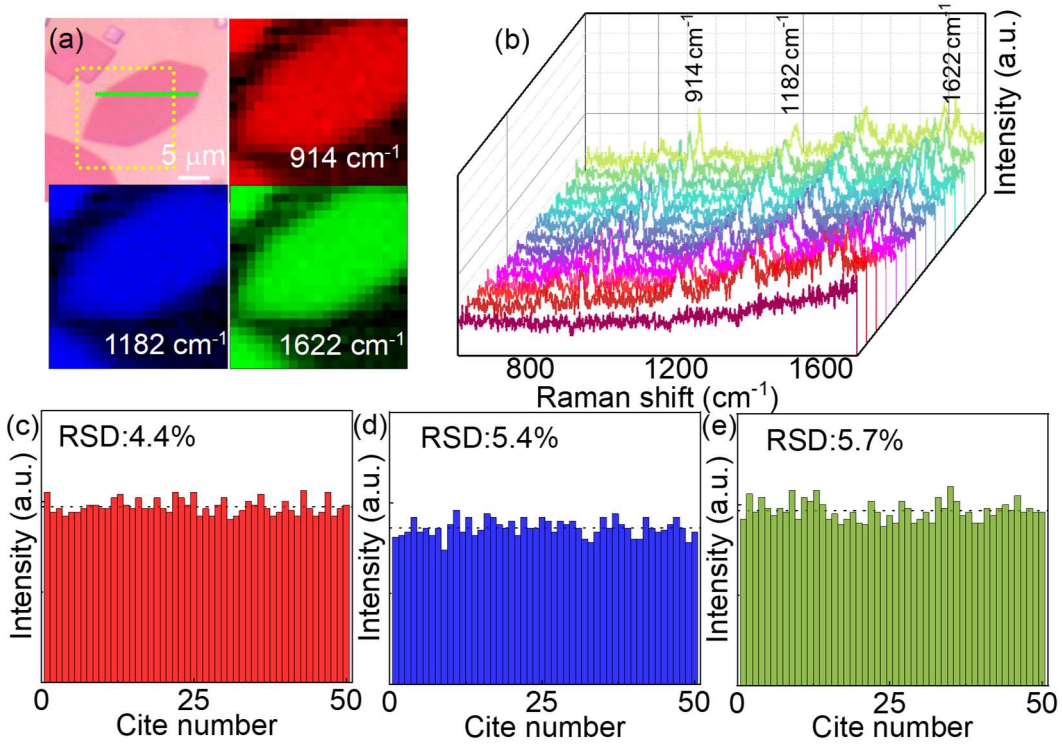

Figure 4. SERS signal uniformity on MoN nanosheets. (a) Optical image of a MoN nanosheet and the Raman mapping based on three typical Raman peaks of methyl violet molecules, the mapping area is marked by yellow dotted square. The scale bar is 10 m. (b) Raman spectra of methyl violet molecules along the green dashed line in panel (a). (c-e) The Raman intensity of three typical peaks 914, 1182 and 1622 cm^{-1} collected from 50 randomly selected points on MoN nanosheets, the calculated RSD are 4.4%, 5.4% and 5.7%, respectively.

3.4. Thickness Dependent SERS Effect of the MoN Nanosheets Substrate

Distinct thickness dependent SERS effect was observed in the MoN nanosheets substrate. MoN nanosheets with different thickness were chosen to collect the Raman spectra after soaking in R6G solution with a concentration of 10^{-7} M. The optical images of the MoN nanosheets are shown in **Figure 5**a. The thickness of those samples was determined by AFM as shown in **Figure S**4, which are 3.9, 4.5, 5, 6.8, 10.2 and 13.6 nm, respectively. The Raman signal intensity decrease with the increasing

Preprints (www.preprints.org) | NOT PEER-REVIEWED | Posted: 7 December 2023 doi:10.20944/preprints202312.0498.v1

of the thickness of the nanosheets, as illustrated in **Figure 5**b. To illustrate it more clearly, the four characteristic Raman peaks of the R6G on different substrate was collected in **Figure 5**c. The intensity of the four Raman peaks decreases with the increasing of the thickness of the MoN nanosheets substrate. To reveal the mechanism of the thickness dependent SERS effect of the MoN substrate, the UV-vis absorption spectroscopy of the MoN substrate was taken as shown in **Figure 5**d. A red-shift of the absorption band with the increasing of the thickness was observed, meanwhile, the absorption band intensity decreases with the increasing of the thickness. As the absorption band of the MoN substrate was ascribed to the surface plasmon resonance, the red-shift and the decrease of intensity can be well explained by the energy loss of the surface plasmon resonance with the increased thickness[43]. The thickness dependent SERS effect of the MoN nanosheets implies that better SERS effect can be achieved with thinner MoN, further effort is worth to take to synthesis thinner MoN nanosheets with larger scale.

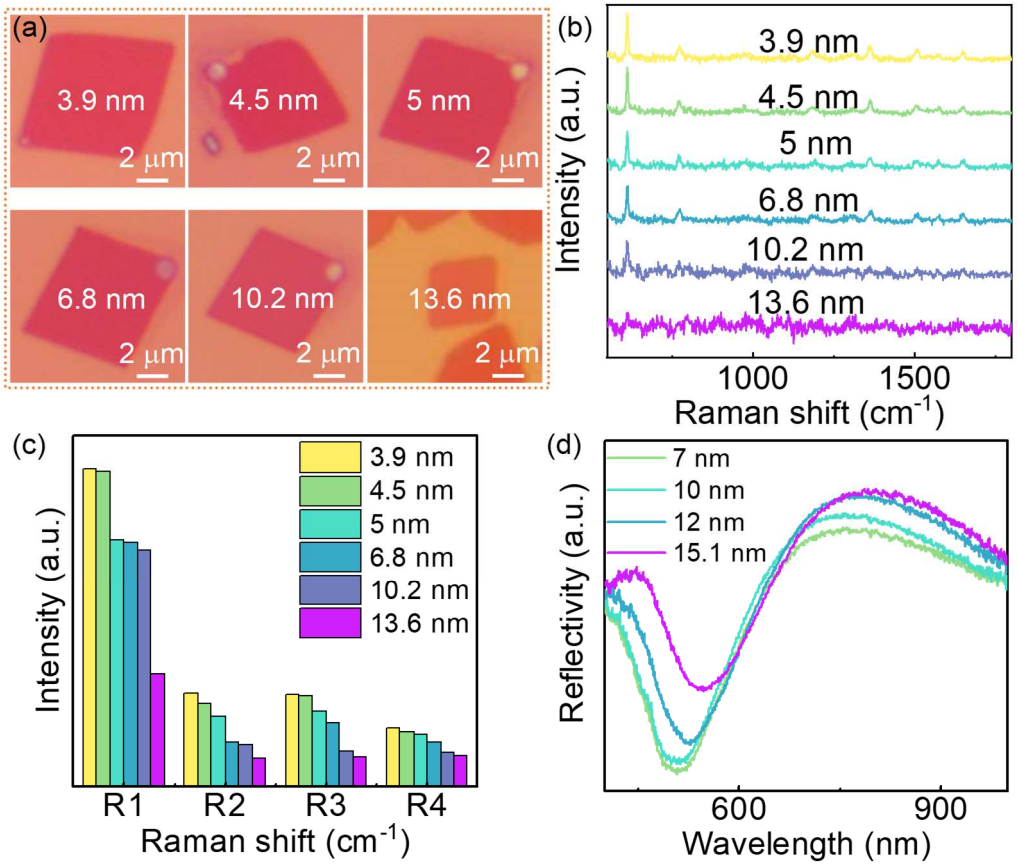

Figure 5. Thickness dependent SERS effect of the MoN nanosheets. (a) Optical microscopy of MoN nanosheets with different thickness. (b) Raman spectra of R6G (10^{-7} M) on MoN substrates with different thickness. (c) Raman intensity of four typical Raman peaks with different thickness. (d) Thickness dependent of UV-vis absorption of MoN nanosheets.

3.5. Thermal Stability of the MoN Nanosheets and Its Reusability for SERS

In addition to high sensitivity, the stability is another important factor for SERS substrate. As shown in **Figure 6**a, the MoN nanosheets show high thermal stability, which can stand for more than 300℃ annealing in air. The maximum tolerable temperature of MoN nanosheets is far larger than the precursor MoO_2 nanosheets.[44] When the annealing temperature increased to 350℃, the color of the nanosheets changes from orange to purple, indicating the oxidation of the nanosheets. The obtained oxide is mainly MoO_3, as indicated by the Raman spectra of the purple nanosheets[45]. When the annealing temperature was below 300℃, the SERS effect preserved well as indicated in **Figure 6**b. Distinct Raman signals of 10^{-6} M R6G can be observed after annealing at 300℃. The high thermal stability of the MoN nanosheets making it possible to be reused as SERS substrate, because heating

Preprints (www.preprints.org) | NOT PEER-REVIEWED | Posted: 7 December 2023 doi:10.20944/preprints202312.0498.v1

was found to be an efficient way to remove molecules from the substrate. Meanwhile, the planar configuration of MoN nanosheets also makes it easier for the absorbed molecule detaching from the surface than those substrate with complex nanostructures. To verify the reusability of the MoN nanosheets SERS substrate, cycle tests of the MoN SERS substrate was performed. As shown in **Figure 6**c, the Raman signal of R6G can be identified after 20 reusing cycles. To illustrate it more clearly, the typical Raman peaks of R6G are shown in **Figure 6**d, no obvious decay of the intensity was observed in both 4 typical Raman peaks.

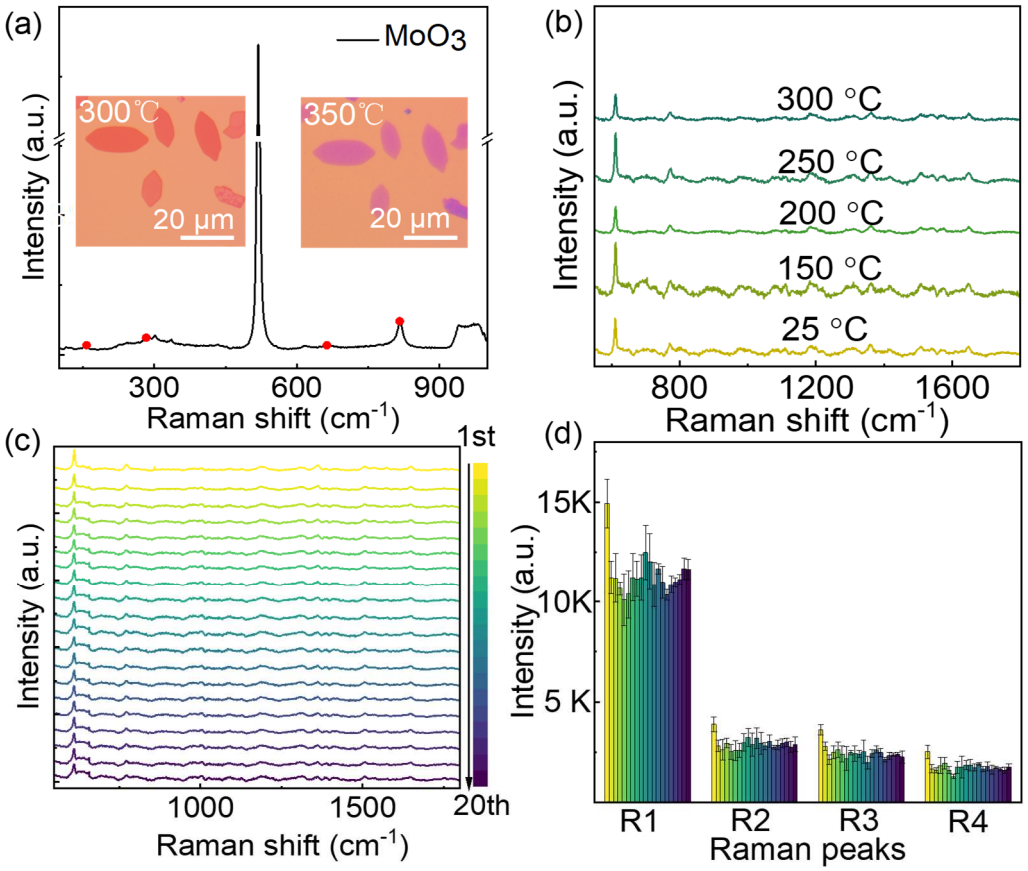

Figure 6. Thermal stability of MoN nanosheets and its reusability as SERS substrate. (a) Optical microscopy images of MoN nanosheets after heating at 300℃ and 350℃ in air for 20 min. The Raman spectra of the purple nanosheets shown characteristic Raman peaks at 156, 300 and 816 cm^{-1}, which are the characteristic Raman peaks of -MoO_3[46]. (b) Raman spectra of R6G (10^{-6} M) on MoN substrates after annealing at different temperature. (c) The Raman spectrum of R6G (10^{-6} M) on the MoN substrates reusing for 20 cycles. (d) Intensity of 4 typical Raman peaks extract from c.

4. Conclusions

In summary, 2D MoN nanosheets was prepared by chemical vapor deposition with their SERS properties studied. The maximum enhancement factor can be 3×10^5 with a limit of detected concentration of 4×10^{-8} M, which is comparable to those noble metal SERS substrates without hot spots. The SERS activity of MoN nanosheets was ascribed to the surface plasmon resonance of the metallic MoN nanosheets, as evidenced by the strong absorption band near 532 nm and the first principle calculation. The planar configuration of MoN nanosheets enable them with excellent Raman signal uniformity within the nanosheets. Meanwhile, distinct thickness dependent sensitivity was observed in the MoN nanosheets SERS substrate, higher sensitivity can be achieved by decreasing the thickness of the nanosheets. Furthermore, MoN nanosheets show high thermal stability, which can be heated in air for more than 300℃ and maintain their SERS activity. Their high stability brings new opportunity as reusable SERS substrates, the SERS sensitivity shown no obvious decay after 20

reusing cycles. The high sensitivity, high stability and Raman signal uniformity, as well as the reusability, making MoN nanosheets an ideal 2D SERS substrate for practical applications.

Supplementary Materials: The following supporting information can be downloaded at the website of this paper posted on Preprints.org. **Figure S1**. Temperature control curves of the growth of MoO_2 nanosheets (a) and during the nitridation process (b). **Figure S2**. Temperature dependent of resistivity of the MoN nanosheets. **Figure S3**. Laser wavelength dependent SERS effect of MoN nanosheets. **Figure S4**. AFM characterization of MoN nanosheets with different thickness. **Figure S5**. Raman spectra of quadrilateral MoN nanosheets and hexagonal MoN nanosheets. **Figure S6**. Optical images of the MoN nanosheets after annealing in air for different temperatures. **Figure S7**. Raman spectra of MoN nanosheets after removing the R6G molecule with methyl alcohol.

Author Contributions: Conceptualization, H.W.; Methodology, H.W. Y.H and M.T.; Investigation, M.T. and P.T.; Resources, H.W. and J.Z.; Calculation, Y.H; Writing – Original Draft Preparation, H.W.; Writing – Review & Editing, H.W. and M.T.; Supervision, H.W. and J.Z.; Project Administration, X.X.; Funding Acquisition, H.W. and J.Z.

Funding: This work was supported by the National Natural Science Foundation of China (Grant Nos. 12002133, 12372109 and 11972171), the Natural Science Foundation of Jiangsu Province (Grant No. BK20200590), the Fundamental Research Funds for the Central Universities (Grant No. JUSRP121040), the 111 project (Grant No. B18027), Open Fund of Key Laboratory for Intelligent Nano Materials and Devices of the Ministry of Education (Grant No. NJ2020003), and the Sixth Phase of Jiangsu Province "333 High Level Talent Training Project" Second Level Talents.

Conflicts of Interest: The authors declare no conflict of interest.

References

1. Cialla-May, D.; Zheng, X. S.; Weber, K.; Popp, J. Recent Progress in Surface-Enhanced Raman Spectroscopy for Biological and Biomedical Applications: From Cells to Clinics. *Chem. Soc. Rev.* **2017**, *46* (13), 3945-3961. DOI: 10.1039/c7cs00172j.
2. Cardinal, M. F.; Vander Ende, E.; Hackler, R. A.; McAnally, M. O.; Stair, P. C.; Schatz, G. C.; Van Duyne, R. P. Expanding Applications of SERS Through Versatile Nanomaterials Engineering. *Chem. Soc. Rev.* **2017**, *46* (13), 3886-3903. DOI: 10.1039/c7cs00207f.
3. Dai, Z. G.; Xiao, X. H.; Wu, W.; Zhang, Y. P.; Liao, L.; Guo, S. S.; Ying, J. J.; Shan, C. X.; Sun, M. T.; Jiang, C. Z. Plasmon-driven Reaction Controlled by the Number of Graphene Layers and Localized Surface Plasmon Distribution During Optical Excitation. *Light-Sci. Appl.* **2015**, *4* (10), e342-e342. DOI: 10.1038/lsa.2015.115.
4. Guo, Y.; Yu, J.; Li, C.; Li, Z.; Pan, J.; Liu, A.; Man, B.; Wu, T.; Xiu, X.; Zhang, C. SERS Substrate Based on the Flexible Hybrid of Polydimethylsiloxane and Silver Colloid Decorated with Silver Nanoparticles. *Opt. Express* **2018**, *26* (17), 21784-21796. DOI: 10.1364/OE.26.021784.
5. Zivanovic, V.; Kochovski, Z.; Arenz, C.; Lu, Y.; Kneipp, J. SERS and Cryo-EM Directly Reveal Different Liposome Structures During Interaction with Gold Nanoparticles. *J. Phys. Chem. Lett.* **2018**, *9* (23), 6767-6772. DOI: 10.1021/acs.jpclett.8b03191.
6. Xu, J.; Li, C.; Si, H.; Zhao, X.; Wang, L.; Jiang, S.; Wei, D.; Yu, J.; Xiu, X.; Zhang, C. 3D SERS Substrate Based on Au-Ag Bi-metal Nanoparticles/MoS_2 Hybrid with Pyramid Structure. *Opt. Express* **2018**, *26* (17), 21546-21557. DOI:10.1364/OE.26.021546.
7. Wu, H.; Zhou, X.; Li, J.; Li, X.; Li, B.; Fei, W.; Zhou, J.; Yin, J.; Guo, W. Ultrathin Molybdenum Dioxide Nanosheets as Uniform and Reusable Surface-Enhanced Raman Spectroscopy Substrates with High Sensitivity. *Small* **2018**, *14* (37). DOI: 10.1002/smll.201802276.
8. Kim, N. J.; Kim, J.; Park, J. B.; Kim, H.; Yi, G. C.; Yoon, S. Direct Observation of Quantum Tunnelling Charge Transfers Between Molecules and Semiconductors for SERS. *Nanoscale* **2019**, *11* (1), 45-49. DOI: 10.1039/c8nr08389d.
9. Zhang, C.; Jiang, S.; Huo, Y.; Liu, A.; Xu, S.; Liu, X.; Sun, Z.; Xu, Y.; Li, Z.; Man, B. SERS Detection of R6G Based on a Novel Graphene Oxide/Silver Nanoparticles/Silicon Pyramid Arrays Structure. *Opt. Express* **2015**, *23* (19), 24811-24821. DOI: 10.1364/OE.23.024811.

10. Zhan, C.; Chen, X. J.; Yi, J.; Li, J. F.; Wu, D. Y.; Tian, Z. Q. From Plasmon-enhanced Molecular Spectroscopy to Plasmon-Mediated Chemical Reactions. *Nat. Rev. Chem.* **2018**, *2* (9), 216-230. DOI: 10.1038/s41570-018-0031-9.
11. Li, J. F.; Zhang, Y. J.; Ding, S. Y.; Panneerselvam, R.; Tian, Z. Q. Core–shell Nanoparticle-Enhanced Raman Spectroscopy. *Chem. Rev.* **2017**, *117* (7), 5002-5069. DOI: 10.1021/acs.chemrev.6b00596.
12. Li, J.; Liu, J.; Yang, Y.; Qin, D. Bifunctional Ag@ Pd-Ag Nanocubes for Highly Sensitive Monitoring of Catalytic Reactions by Surface-enhanced Raman Spectroscopy. *J. Am. Chem. Soc.* **2015**, *137* (22), 7039-7042. DOI: 10.1021/jacs.5b03528.
13. Jiang, T.; Chen, G.; Tian, X.; Tang, S.; Zhou, J.; Feng, Y.; Chen, H. Construction of Long Narrow Gaps in Ag Nanoplates. *J. Am. Chem. Soc.* **2018**, *140* (46), 15560-15563. DOI: 10.1021/jacs.8b06969.
14. Shen, W.; Lin, X.; Jiang, C.; Li, C.; Lin, H.; Huang, J.; Wang, S.; Liu, G.; Yan, X.; Zhong, Q. Reliable Quantitative SERS Analysis Facilitated by Core–shell Nanoparticles with Embedded Internal Standards. *Angew. Chem. Int. Edit.* **2015**, *54* (25), 7308-7312. DOI: 10.1002/anie.201502171.
15. Vantasin, S.; Ji, W.; Tanaka, Y.; Kitahama, Y.; Wang, M.; Wongravee, K.; Gatemala, H.; Ekgasit, S.; Ozaki, Y. 3D SERS Imaging Using Chemically Synthesized Highly Symmetric Nanoporous Silver Microparticles. *Angew. Chem. Int. Edit.* **2016**, *128* (29), 8531-8535. DOI: 10.1002/anie.201603758.
16. Langer, J.; Jimenez, D. A. D.; Aizpurua, J.; Alvarez-Puebla, R. A.; Auguié, B.; Baumberg, J. J.; Bazan, G. C.; Bell, S. E.; Boisen, A.; Brolo, A. G. Present and Future of Surface-enhanced Raman Scattering. *ACS Nano* **2019**, *14* (1), 28-117. DOI: 10.1021/ACSNANO.9B04224.
17. Li, J.; Yi, W.; Li, Y.; Liu, W.; Bai, H.; Jiao, Z.; Zhang, Y.; Wang, X.; Zou, M.; Xi, G. Nitrogen-doped Titanium Monoxide Flexible Membrane for a Low-cost, Biocompatible, and Durable Raman Scattering Substrate. *Anal. Chem.* **2021**, *93* (37), 12776-12785. DOI: 10.1021/acs.analchem.1c02971.
18. Li, Y.; Bai, H.; Zhai, J.; Yi, W.; Li, J.; Yang, H.; Xi, G. Alternative to Noble Metal Substrates: Metallic and Plasmonic Ti_3O_5 Hierarchical Microspheres for Surface Enhanced Raman Spectroscopy. *Anal. Chem.* **2019**, *91* (7), 4496-4503. DOI: 10.1021/acs.analchem.8b05282.
19. Zheng, Z.; Cong, S.; Gong, W.; Xuan, J.; Li, G.; Lu, W.; Geng, F.; Zhao, Z. Semiconductor SERS Enhancement Enabled by Oxygen Incorporation. *Nat. Commun.* **2017**, *8* (1), 1993. DOI: 10.1038/s41467-017-02166-z.
20. Jiang, L.; You, T.; Yin, P.; Shang, Y.; Zhang, D.; Guo, L.; Yang, S. Surface-Enhanced Raman Scattering Spectra of Adsorbates on Cu_2O Nanospheres: Charge-Transfer and Electromagnetic Enhancement. *Nanoscale* **2013**, *5* (7), 2784-2789. DOI: 10.1039/c3nr33502j.
21. Gordon, T. R.; Cargnello, M.; Paik, T.; Mangolini, F.; Weber, R. T.; Fornasiero, P.; Murray, C. B. Nonaqueous Synthesis of TiO_2 Nanocrystals Using TiF4 to Engineer Morphology, Oxygen Vacancy Concentration, and Photocatalytic Activity. *J. Am. Chem. Soc.* **2012**, *134* (15), 6751-6761. DOI: 10.1021/ja300823a.
22. Han, S. Y.; Guo, Q. H.; Xu, M. M.; Yuan, Y. X.; Shen, L. M.; Yao, J. L.; Liu, W.; Gu, R. A. Tunable Fabrication on Iron Oxide/Au/Ag Nanostructures for Surface Enhanced Raman Spectroscopy and Magnetic Enrichment. *J. colloid interf. Sci.* **2012**, *378* (1), 51-57. DOI: 10.1016/j.jcis.2012.04.047.
23. Zhang, Q.; Li, X.; Ma, Q.; Zhang, Q.; Bai, H.; Yi, W.; Liu, J.; Han, J.; Xi, G. A Metallic Molybdenum Dioxide with High Stability for Surface Enhanced Raman Spectroscopy. *Nat. Commun.* **2017**, *8*, 14903. DOI: 10.1038/ncomms14903.
24. Xie, L.; Ling, X.; Fang, Y.; Zhang, J.; Liu, Z. Graphene as a Substrate to Suppress Fluorescence in Resonance Raman Spectroscopy. *J. Am. Chem. Soc.* **2009**, *131* (29), 9890-9891. DOI: 10.1021/ja9037593.
25. Santhoshkumar, S.; Wei, W. S.; Madhu, M.; Tseng, W. B.; Tseng, W. L. Chemically Engineered Sulfur Vacancies on Few-Layered Molybdenum Disulfide Nanosheets for Remarkable Surface-Enhanced Raman Scattering Activity. *J. Phys. Chem. C* **2023**, *127* (18), 8803-8813. DOI: 10.1021/acs.jpcc.3c01044.
26. Cai, Q.; Mateti, S.; Yang, W.; Jones, R.; Watanabe, K.; Taniguchi, T.; Huang, S.; Chen, Y.; Li, L. H. Boron Nitride Nanosheets Improve Sensitivity and Reusability of Surface-Enhanced Raman Spectroscopy. *Angew. Chem. Int. Edit.* **2016**, *55* (29), 8405-8409. DOI: 10.1002/anie.201600517.
27. Lin, X. M.; Cui, Y.; Xu, Y. H.; Ren, B.; Tian, Z. Q. Surface-Enhanced Raman Spectroscopy: Substrate-Related Issues. *Anal. Bioanal. Chem.* **2009**, *394*, 1729-1745.
28. Xie, J.; Xie, Y. Transition Metal Nitrides for Electrocatalytic Energy Conversion: Opportunities and Challenges. *Chem. Eur. J.* **2016**, *22* (11), 3588-3598. DOI: 10.1002/chem.201501120.
29. Anasori, B.; Lukatskaya, M. R.; Gogotsi, Y. 2D Metal Carbides and Nitrides (MXenes) for Energy Storage. *Nat. Rev. Mater.* **2017**, *2* (2), 1-17. DOI: 10.1038/natrevmats.2016.98.

30. Khazaei, M.; Arai, M.; Sasaki, T.; Chung, C. Y.; Venkataramanan, N. S.; Estili, M.; Sakka, Y.; Kawazoe, Y. Novel Electronic and Magnetic Properties of Two-Dimensional Transition Metal Carbides and Nitrides. *Adv. Funct. Mater.* **2013**, *23* (17), 2185-2192. DOI: 10.1002/adfm.201202502.
31. Yuan, Y.; Wang, J.; Adimi, S.; Shen, H.; Thomas, T.; Ma, R.; Attfield, J. P.; Yang, M. Zirconium Nitride Catalysts Surpass Platinum for Oxygen Reduction. *Nat. Mater.* **2020**, *19* (3), 282-286. DOI: 10.1038/s41563-019-0535-9.
32. Zhong, Y.; Xia, X.; Shi, F.; Zhan, J.; Tu, J.; Fan, H. J. Transition Metal Carbides and Nitrides in Energy Storage and Conversion. *Adv. Sci.* **2016**, *3* (5), 1500286. DOI: 10.1002/advs.201500286.
33. Mojtabavi, M.; VahidMohammadi, A.; Liang, W.; Beidaghi, M.; Wanunu, M. Single-Molecule Sensing Using Nanopores in Two-Dimensional Transition Metal Carbide (MXene) Membranes. *ACS Nano* **2019**, *13* (3), 3042-3053. DOI: 10.1021/acsnano.8b08017.
34. Guan, H. M.; Yi, W. C.; Li, T.; Li, Y. H.; Li, J. F.; Bai, H.; Xi, G. C. Low Temperature Synthesis of Plasmonic Molybdenum Nitride Nanosheets for Surface Enhanced Raman Scattering. *Nat. Commun.* **2020**, *11* (1), 3889. DOI: 10.1038/s41467-020-17628-0.
35. Song, X.; Li, J.; Kong, Q.; Bai, H.; Xi, G. Molybdenum Nitride Porous Prisms with a Strong Plasmon Resonance Effect in the Visible Region for Surface-Enhanced Raman Spectroscopy. *J. Phys. Chem. Lett.* **2022**, *13* (29), 6777-6782. DOI: 10.1021/acs.jpclett.2c01558.
36. Du, R.; Yi, W.; Li, W.; Yang, H.; Bai, H.; Li, J.; Xi, G. Quasi-Metal Microwave Route to MoN and Mo(2)C Ultrafine Nanocrystalline Hollow Spheres as Surface-Enhanced Raman Scattering Substrates. *ACS Nano* **2020**, *14* (10), 13718-13726. DOI: 10.1021/acsnano.0c05935.
37. Wang, Y.; Jian, C.; Hong, W.; Liu, W. Nonlayered 2D Ultrathin Molybdenum Nitride Synthesized Through the Ammonolysis of 2D Molybdenum Dioxide. *Chem. Commun.* **2021**, *57* (2), 223-226. DOI: 10.1039/d0cc07065c.
38. Gao, H.; Cao, J.; Li, T.; Luo, W.; Gray, M.; Kumar, N.; Burch, K. S.; Ling, X. Phase-Controllable Synthesis of Ultrathin Molybdenum Nitride Crystals Via Atomic Substitution of MoS_2. *Chem. Mater.* **2021**, *34* (1), 351-357. DOI: 10.1021/acs.chemmater.1c03712.
39. Luther, J. M.; Jain, P. K.; Ewers, T.; Alivisatos, A. P. Localized Surface Plasmon Resonances Arising from Free Carriers in Doped Quantum Dots. *Nat. Mater.* **2011**, *10* (5), 361-366. DOI: 10.1038/nmat3004.
40. Hildebrandt, P.; Stockburger, M. Surface-Enhanced Resonance Raman Spectroscopy of Rhodamine 6G Adsorbed on Colloidal Silver. *J. Phys. Chem.* **1984**, *88* (24), 5935-5944. DOI:10.1021/j150668a038.
41. Cong, S.; Yuan, Y.; Chen, Z.; Hou, J.; Yang, M.; Su, Y.; Zhang, Y.; Li, L.; Li, Q.; Geng, F.; et al. Noble Metal-Comparable SERS Enhancement from Semiconducting Metal Oxides by Making Oxygen Vacancies. *Nat. Commun.* **2015**, *6*, 7800. DOI: 10.1038/ncomms8800.
42. Xu, W.; Ling, X.; Xiao, J.; Dresselhaus, M. S.; Kong, J.; Xu, H.; Liu, Z.; Zhang, J. Surface Enhanced Raman Spectroscopy on a Flat Graphene Surface. *P. Natl. A. Sci.* **2012**, *109* (24), 9281-9286. DOI: 10.1073/pnas.1205478109.
43. Raether, H. Surface Plasma Oscillations as a Tool for Surface Examinations. *Surf. Sci.* **1967**, *8* (1), 233-246. DOI: 10.1016/0039-6028(67)90085-4.
44. Li, J.; Yin, J.; Li, X.; Zhou, J.; Guo, W. Chemical Vapor Deposition of Ultra-Thin Molybdenum Dioxide Nanosheets. *Mater. Lett.* **2016**, *174*, 188-191. DOI: 10.1016/j.matlet.2016.03.081.
45. Camacho-López, M. A.; Escobar-Alarcón, L.; Picquart, M.; Arroyo, R.; Córdoba, G.; Haro-Poniatowski, E. Micro-Raman Study of the m-MoO_2 to α-MoO_3 Transformation Induced by CW-laser Irradiation. *Opt. Mater.* **2011**, *33* (3), 480-484. DOI: 10.1016/j.optmat.2010.10.028.
46. Windom, B. C.; Sawyer, W.; Hahn, D. W. A Raman Spectroscopic Study of MoS_2 and MoO_3: Applications to Tribological Systems. *Tribol. Lett.* **2011**, *42*, 301-310. DOI:10.1007/s11249-011-9774-x.